Sensor and Simulation Notes

Note 364

January 1994

Experimental Validation of IRA Models

Everett G. Farr
Farr Research
Consultant to Mission Research Corporation

C. Jerald Buchenauer
Phillips Laboratory

Abstract

We present here data taken on a large tabletop transient antenna range to characterize lens IRAs, reflector IRAs, and TEM horns. Comparisons are made to simple analytical models. Based on these preliminary results, we find good agreement between our experiments and the theory.

I. Introduction

Considerable effort has gone into developing models for reflector Impulse Radiating Antennas (IRAs), lens IRAs, and TEM horns [1-13]. However, experimental data verifying the models has not yet appeared. In this note we provide measurements of these antennas, and we compare our results to theory.

The types of antennas to be characterized are shown in Figure 1.1. Reflector IRAs consist of a TEM feed and a paraboloidal reflector. The feed is terminated to the reflector in an impedance which provides a cardioid pattern at low frequencies. Lens IRAs consist of TEM horns with a lens in their aperture, to focus the radiated field. All of our measurements were taken on a ground plane, so only half of the antenna was tested.

We begin this note by summarizing the theories tested with the experiments. We then provide a detailed description of our measurements and compare to the theory.
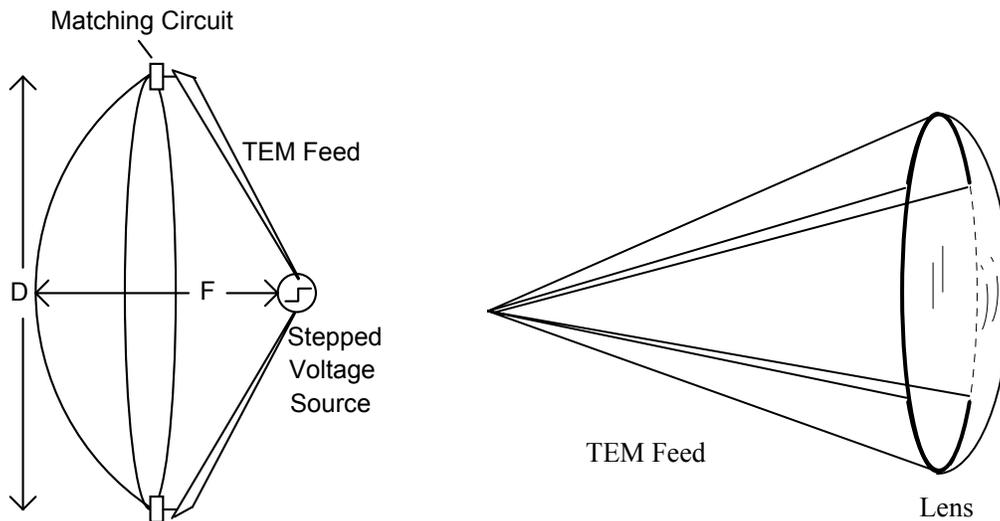

Figure 1.1. A reflector IRA, left, and a lens IRA, right.

II. Antenna and Sensor Theory

We provide here a general review of the theories of operation of the antenna and sensor we are checking with this experiment.

A. Reflector IRA

The field radiated on boresight for the reflector IRA has been documented in [1,7]. For high impedance feeds (about 400 ohms or higher) the radiated field on boresight is, to a first approximation,

$$E(r,t) \;=\; \frac{D}{4\pi r c f_g}\left\{\frac{dv(t-2F/c)}{dt} - \frac{c}{2F}\left[v(t)-v(t-2F/c)\right]\right\} \tag{2.1}$$

where D is the diameter of the reflector, F is the focal length, $f_g = Z_{feed}/Z_o$, $Z_o = 376.727\ \Omega$, $v(t)$ is the driving voltage, c is the speed of light, and r is the distance away from the antenna on boresight. Corrections are necessary for feed blockage, as provided in [11]. When the feed impedance is 400 Ω (or 200 Ω for a half antenna), the correction is 20 percent, and this will be used in the experimental cases we analyze.

We can write the above equation as a step response, assuming $v(t) = V\,u(t)$, where $u(t)$ is the Heaviside step function. With this assumption, the radiated far field on boresight is

$$E(r,t) \;=\; \frac{V}{r}\frac{D}{4\pi c f_g}\left\{\delta_a(t-2F/c) - \frac{c}{2F}\left[u(t)-u(t-2F/c)\right]\right\} \tag{2.2}$$

where $\delta_a(t)$ is the approximate delta function as defined in [2,4]. A diagram of this step response is shown in Figure 2.1. Note that there is also a tail in the step response that is not yet well understood.
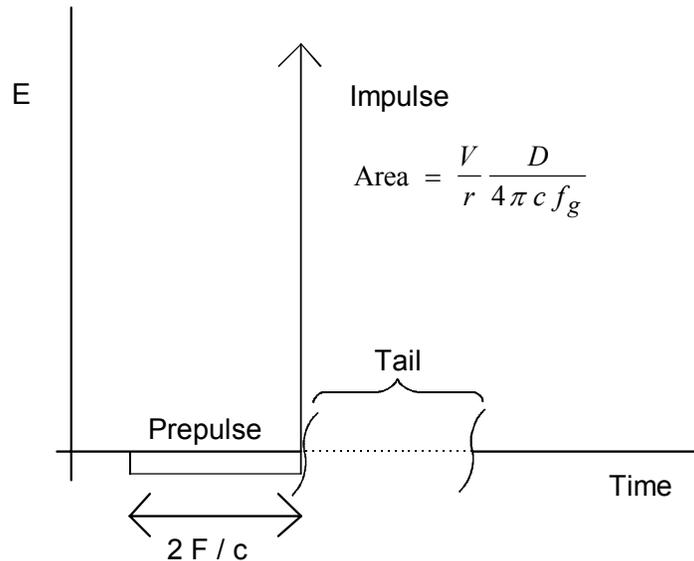

Figure 2.1. Step response of reflector IRA on boresight.

B. Lens IRAs and Long TEM Horns

Next, we consider the lens IRA, or if the horn is long enough, a TEM horn without a lens. Consider first a long TEM horn, as shown in Figure 2.2. If one assumes that the aperture fields are focused, as would be approximately true for a very long horn, then the model for the radiated field on boresight is

$$E(r,t) = -\frac{h}{4\pi r c f_g}\left[\frac{dv(t)}{dt} - \frac{c}{2\ell}\left[v(t) - v(t - 2\ell/c)\right]\right] \tag{2.3}$$

where f_g is the feed impedance normalized to the impedance of free space, and h is the height of the aperture. Note that in [8] this model was further modified by defocusing the aperture. This is unnecessary for lens IRAs, since the aperture field is in focus.
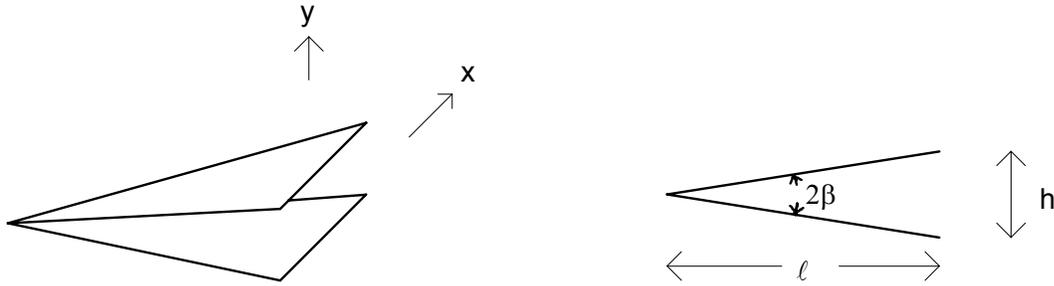

Figure 2.2. A simple TEM horn.

It is also useful to express this in terms of the step response. If the driving voltage in the above equation is $v(t)=Vu(t)$, then the step response of the lens IRA is

$$E(r,t) = -\frac{V}{r}\frac{h}{4\pi c f_g}\left[\delta_a(t) - \frac{c}{2\ell}\left[u(t) - u(t - 2\ell/c)\right]\right] \tag{2.4}$$

where $u(t)$ is the Heaviside step function $\delta_a(t)$ is the approximate delta function. A diagram of this is shown in Figure 2.3.

The figure shows E_z on the vertical axis and t_r (Retarded time) on the horizontal axis. Labels include:

$$\text{Impulse Area} \; = \; \frac{V}{r}\,\frac{h}{4\pi c\,f_g}$$

$$\frac{V}{r}\,\frac{h}{8\pi \ell f_g}$$
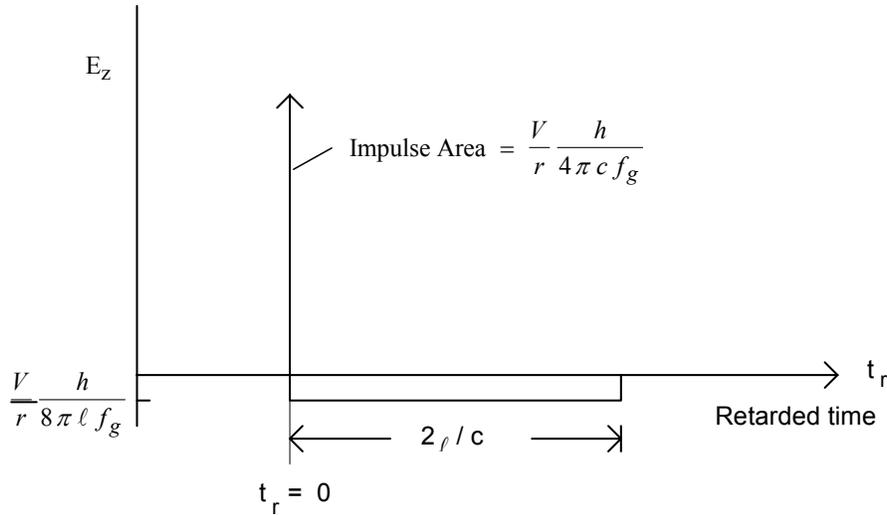
$$2\ell / c$$

$$t_r = 0$$

Figure 2.3. Step response of a lens IRA or long TEM horn.

This model requires a few modifications in order to apply it to lens IRAs as shown in Figure 1.1. First, note that the height of the aperture is ambiguous because the aperture shape consists of curved plates rather than flat. To be rigorous, the new aperture height must be calculated either from the line dipole moment of the aperture or from the field at the center of the aperture. A reasonable approximation is just to assume an average height based on the minimum and maximum separations of the curved plates. Thus, where h is called for in the following formulas, we will use $D(1+1/\sqrt{2})/2 = 0.854\,D$, where D is the diameter of the circular aperture.

Note also that the theory we have just described has been derived for an infinite aperture. However, in our case, only the fields within the aperture are focused, so we wish to just include those in the analysis. It turns out that for our particular configuration of a circular aperture with curved plates the fields outside the circular aperture make no net contribution to the total field on boresight. This is a result of the theory of circular apertures, as described in [10], and the theory of self-reciprocal apertures, as described in [12]. Thus, for our particular configuration of lens IRA, equation (2.4) is equally valid for a circular aperture and for an infinite aperture.

Finally, we note that reflections from the lens have not been taken into account. This will reduce the transmitted field by four percent for polyethylene lenses, which have a relative dielectric constant of 2.3.

C. TEM Horns

If we now remove the lens from the lens IRA, we then have a TEM horn. The step response of a TEM horn is generated by " flattening" the approximate delta function in the step response for the lens IRA above. This is shown in Figure 2.4, and it comes from the fact that at very early times the step response is simply that of an infinite cone. Note that E_y^{norm} in Figure 2.4 is the field in the center of the aperture normalized to V/h. As such, it is approximately equal to unity, and to first order can be ignored.

5

E-field

$\frac{V}{r}\frac{\ell}{h}E_y{}^{norm}$

$t_c \cong \dfrac{h^2}{8\,\ell\,c}$

$t_a = \dfrac{h^2}{4\,\pi\,c\,f_g\,\ell\,E_y{}^{norm}}$

$\frac{V}{r}\frac{h}{8\,\pi\,f_g\,\ell}$
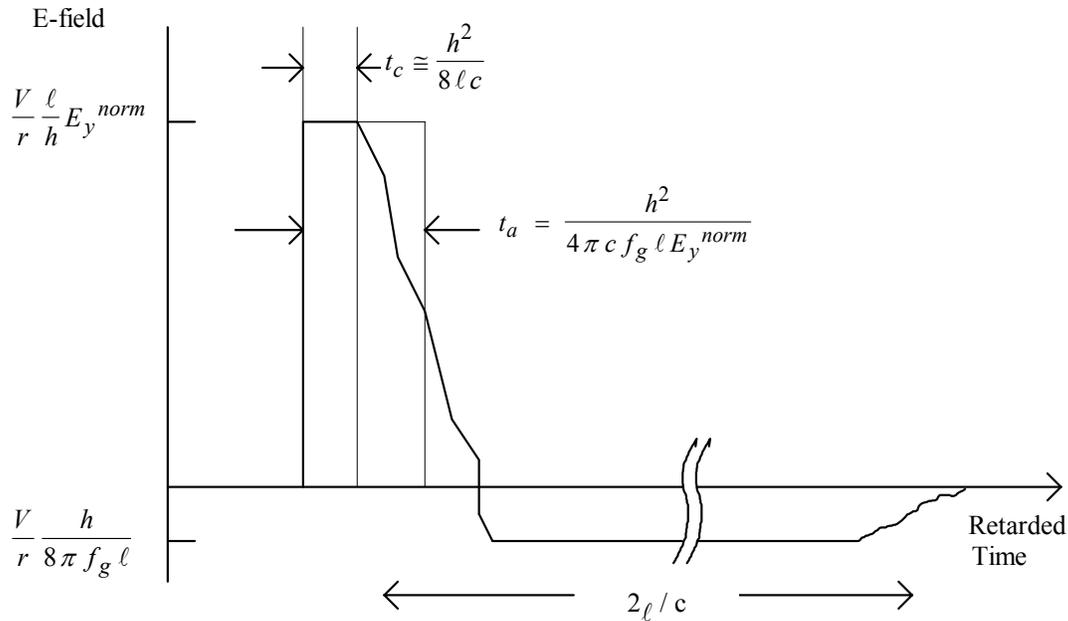
Retarded
Time

$2_\ell / c$

Figure 2.4. Step response of a TEM horn, with a "flattened" delta function.

In order to obtain a bandwidth-limited step response from the above step response, one must convolve the step response with the derivative of the driving voltage. We have assumed that the derivative of the driving voltage is a Gaussian waveform as described in [9], whose integral has a 10-90% risetime of 100 ps.

The above step response merely specifies many of the parameters, without identifying a specific waveshape. However, we have to choose an actual waveform in order to carry out the convolution. Thus, we approximate the step response as a squared-off version of the above step response of the TEM horn (Figure 2.5).
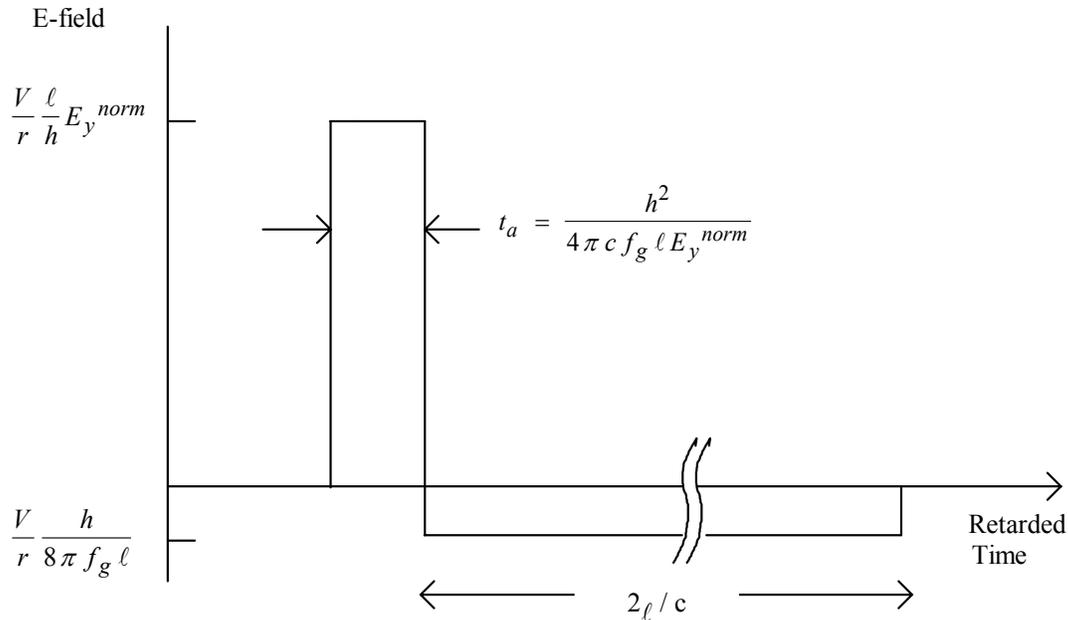
E-field

$\frac{V}{r}\frac{\ell}{h}E_y{}^{norm}$

$t_a = \dfrac{h^2}{4\,\pi\,c\,f_g\,\ell\,E_y{}^{norm}}$

$\frac{V}{r}\frac{h}{8\,\pi\,f_g\,\ell}$

Retarded
Time

$2_\ell / c$

Figure 2.5. Approximate step response of a TEM horn.

6

D. The Replicating Sensor

When choosing the sensor for these experiments, one must decide how to integrate the received signal. Ordinarily one would use a B-dot or D-dot sensor, and implement either a hardware or software integration of the received signal. However, the sensor used in this experiment was a novel design that responded to the incident electric field, rather than its derivative (Figure 2.6). This class of sensors is called "Limited-Angle-of-Incidence and Limited-Time Electric Sensors," and their behavior is described in [14]. By using this class of sensor, the integration is avoided.
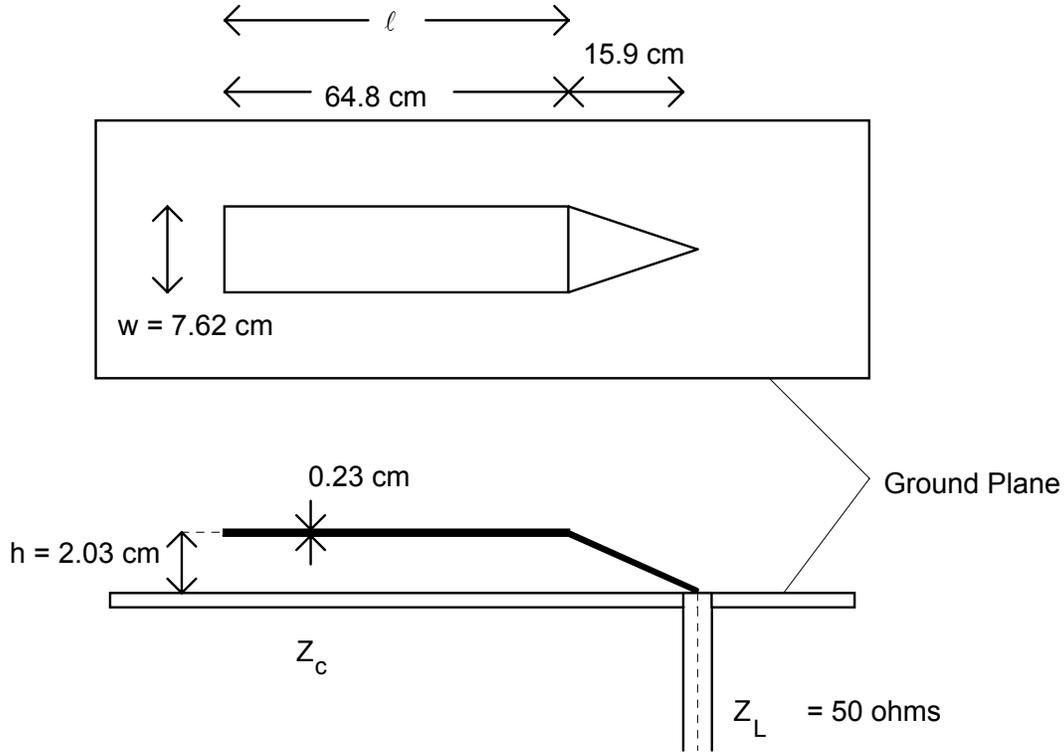
Figure 2.6. The replicating sensor

We can express the response of this sensor in terms of an effective height, which is the ratio of the voltage out of the sensor to the incident electric field. Thus, the effective height is

$$h_{eff} \quad = \quad \frac{V_{meas}}{E_{inc}} \quad = \quad h\frac{Z_L}{Z_c + Z_L} \tag{2.5}$$

where h is the distance from the ground plane to the center of the thick plate. This approximation is valid for two transit times of the sensor, or for a time $2\ell/c$. Note that the response of this sensor is actually more complicated than this, and will require further study. Nevertheless, the accuracy of this model should be sufficient for our purposes.

7

The impedance of the sensor, Z_c, can be found either from analysis or from measurement. This impedance can be calculated approximately by using the techniques in [15], if one assumes that the plates are thin. The cross section of the transmission line is shown in Figure 2.7. For our case, b/a is about 0.5, so the impedance of the whole transmission line (both halves) is 115.4 Ω, according to [15 (Table 4.1)]. Since we only use half of the transmission line, the impedance is 57.7 Ω. This was confirmed by measuring the impedance with a TDR, where an impedance of 57 Ω was observed. At this point, one must choose whether to use the experimental value or the predicted value for Z_c. Noting that it makes only one percent difference in the effective height, we chose the experimental value of $Z_c = 57$ Ω. Thus, the effective height of our sensor is

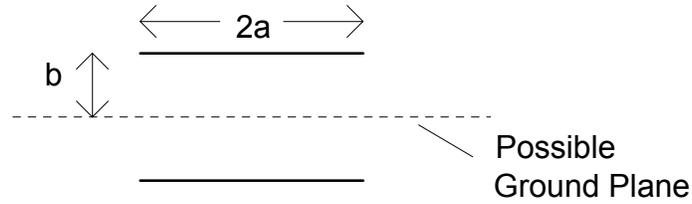$$h_{eff} = 0.95 \ \text{cm} \tag{2.6}$$

Figure 2.7. Cross section of the transmission line in the replicating sensor.

E. The Driving Voltage

The driving voltage is approximated by a 40 V integrated Gaussian waveform with a 10-90 percent risetime of 80 ps. Some degradation in the risetime is evident in the radiated field, so a risetime of 100 ps was used in the calculations. The derivative of the waveform is Gaussian in form and is expressed as [9]

$$\frac{dv(t)}{dt} = \frac{V}{\sqrt{2\pi}\ \sigma}\ e^{-(t/\sigma)^2/2} \tag{2.7}$$
$$\sigma = t_{10-90}\ /\ 2.56$$

In this equation, t_{10-90} is the 10-90 percent risetime of $v(t)$, and V is the peak voltage of $v(t)$, or in our case 40 V. Note that there is an impedance mismatch at the feed point of the antenna under test, which must be taken into account.

F. Mismatch at the Feed Point

It was necessary to take into account the mismatch at the feed point, since the antennas did not have a 50 Ω input impedance. The formula for the voltage launched onto the antenna is

$$V_{ant} = \tau V_{inc} , \qquad \tau = \frac{2Z_{feed}}{Z_{feed} + 50 \, \Omega} \qquad (2.8)$$

where V_{inc} is the magnitude of the incident step voltage on the feed cable. For the reflector IRA, $Z_{feed} = 200 \, \Omega$, and for the TEM horn (with or without the lens) $Z_{feed} = 94.25 \, \Omega$.

G. Lens Design

The lens was designed so that all rays would travel the same electrical length out to a planar aperture. One surface was flat, and the shape of the second surface was calculated numerically. This constitutes a rigorous high-frequency design.

III.   Experimental Configuration

A. The Antennas

Three antennas were tested. The dimensions for the lens IRA are shown in Figure 3.1. The lens IRA was tested both with and without the lens. When tested without the lens, this is just a TEM horn. The lens was made of polyethylene, with a relative dielectric constant of 2.3. The two antennas were also tested both with and without an aperture plate, in order to see its effect. The input impedance of the feed is $Z_o/4 = 94.25\ \Omega$, which is thought to provide the optimal output. This feed impedance provides maximum field uniformity at the center of the aperture, as shown in [16]. This value of feed impedance would have to be doubled for a whole antenna (both halves).
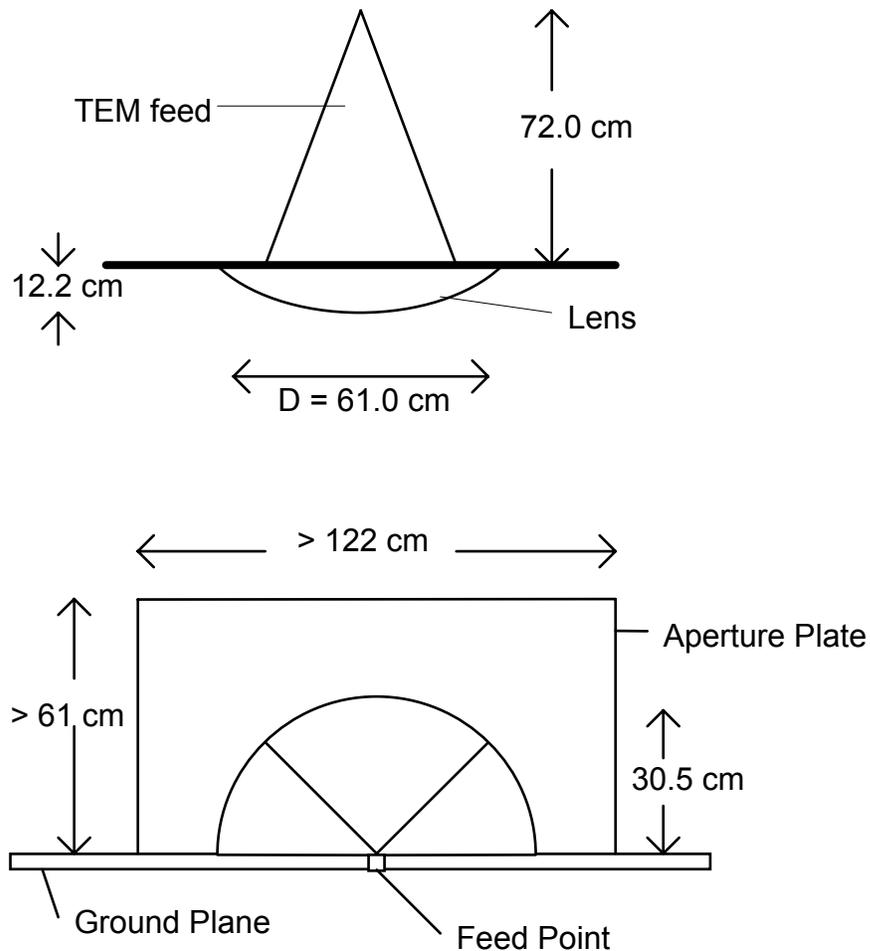
Figure 3.1. The lens IRA studied in this experiment.

The reflector IRA is shown in Figure 3.2. The input impedance for a half antenna is 200 Ω, which would correspond to 400 Ω for a full antenna. Note that the feed is in the " facing plates" configuration, using the terminology of [11]. The feed arms were shorted to the reflector, so the low-frequency portion of the signal could not be tested. Hopefully, a later measurement will test the low-frequency behavior of this antenna using a matching circuit at the junction.
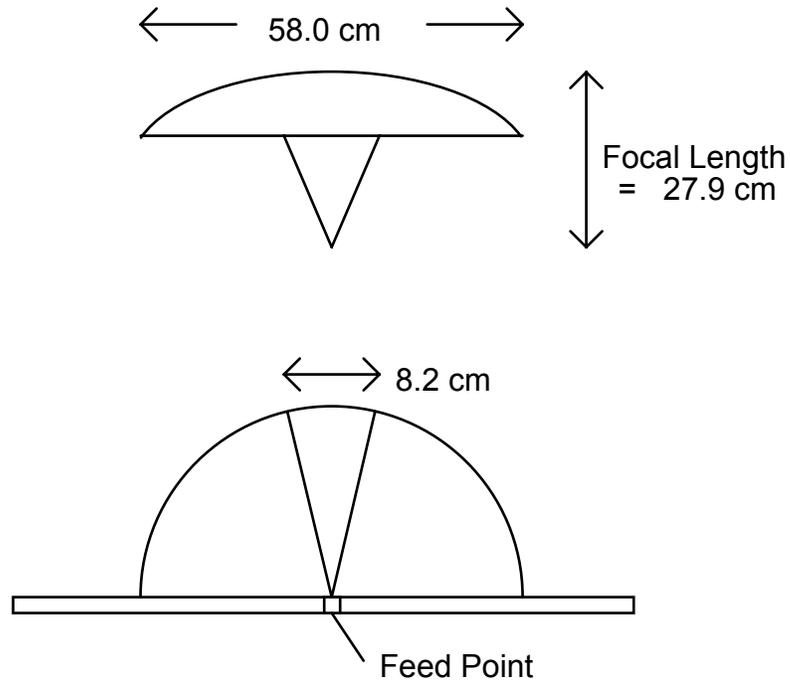
Figure 3.2. The reflector IRA studied in this experiment

B. Instrumentation

A diagram of the testing table is shown in Figure 3.3. The pulser (Picosecond Pulse Labs 4000B) sends a pretrigger to the sampling scope . The pulser has a peak voltage of 35-40 V and a 10–90 percent risetime somewhere between 80 and 100 ps. The device under test radiated across the ground plane and the signal was received by a " limited time, limited angle of incidence" sensor. The dimensions of the sensor were shown in the previous section of this report. The signal was recorded by a 7000 series Tektronix sampling scope with a 7S11 sampling scope plugin, a 7T11 timebase plugin, and an S-4 sampling head with 25 ps. risetime.
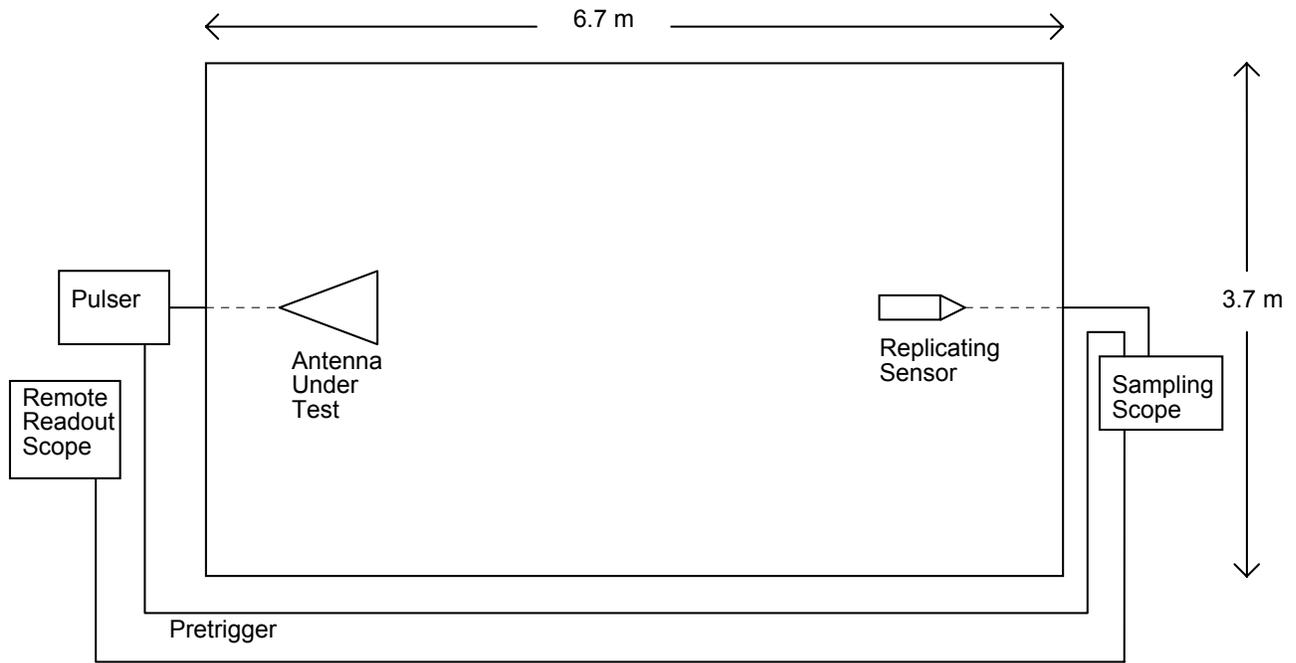
Figure 3.3. The experimental test setup

C. Feed Point Locations

Some issues concerning the location of the feed point must be clarified, in order to determine the distance from the antenna under test to the sensor. The layout for the TEM horn and lens IRA experiments is shown in Figure 3.4. The distances shown are the values of r used in the analysis formulas.
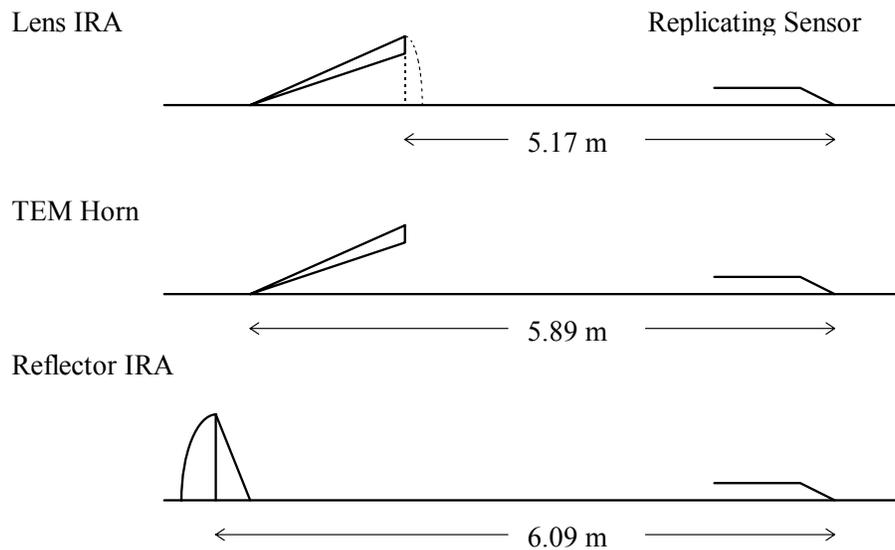

Figure 3.4. Distances used for comparing experimental results to calculations.

IV.   Results

The measured results for the Lens IRA and TEM horn are shown in Figures 4.1 and 4.2. For the lens IRA, we predicted a peak of 56.5 V/m and observed 59.9 V/m. For the TEM horn, we predicted a peak of 24.4 V/m, and observed 27.3 V/m. Our predictions were therefore low by 6% and 12%, respectively. Note that if our theory had included reflections from the lens, this would have reduced the prediction for the lens IRA by an additional 4%. This is reasonable agreement considering the approximations used in the theory and the uncertainties in the measurements.

The measured results for the reflector IRA are shown in Figure 4.3, and the predictions are shown in Figure 4.4. We predicted a peak of 30.1 V/m and we measured a peak of 25.2 V/m. For this case our predictions are 16% too high. Thus, the agreement here is not quite as good.

The primary reason for the problem with the reflector IRA prediction is feed blockage. This effect was calculated in [11(Figure 4.5)], and it was shown to reduce the magnitude of the impulse portion of the step response by 20% for a feed impedance of 400 Ω. We can modify our model by reducing the impulse magnitude by 20%, and we obtain much better agreement (Figure 4.5). With the adjustment, the field is calculated to be 23.9 V/m, which is lower than the observed peak by 5%. Note that our model now has the property that the net area of the radiated field is not equal to zero. Additional terms due to diffraction from the reflector and the feed arms account for the balance of the waveform, but the theory of these additional terms is not yet complete. This second model is the preferred model, however, one must understand its limitations.

When we use our best models, our predicted fields are low by between 5% and 12%. This could be accounted for by a using a slightly faster risetime in the experiments than in the predictions. Recall that in the predictions we used a risetime of 100 ps, which assumed a small amount of degradation from the 80 ps rating of the device. If the risetime were 90 ps, then our predictions would all increase by 10%, giving better correlation with the measurements.

Note that there is some undershoot in the measured waveform of the reflector IRA after the impulse, which is not explicitly predicted by the theory. This is likely caused by diffraction either from the edge of the reflector, or from the edge of the feed arms.

Finally, we consider the effect of the aperture plate in a Lens IRA or TEM horn (Figure 4.6). We had felt that the aperture plate would make little difference to the early-time response, and we found that to be the case. For the lens IRA, the peak is reduced by 7% with the aperture plate in place. For the TEM horn, the peak is reduced by 4% with the aperture plate.
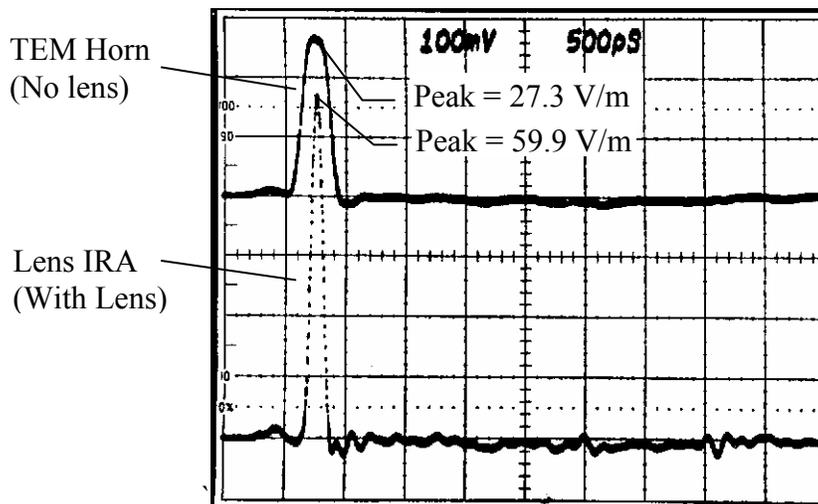
Figure 4.1 Experimental results for TEM horn and lens IRA. Note that the scales are 500 ps/division horizontal and 100 mV/division vertical. Since the effective height of the sensor is 0.95 cm, this corresponds to 10.5V/m/division vertical.
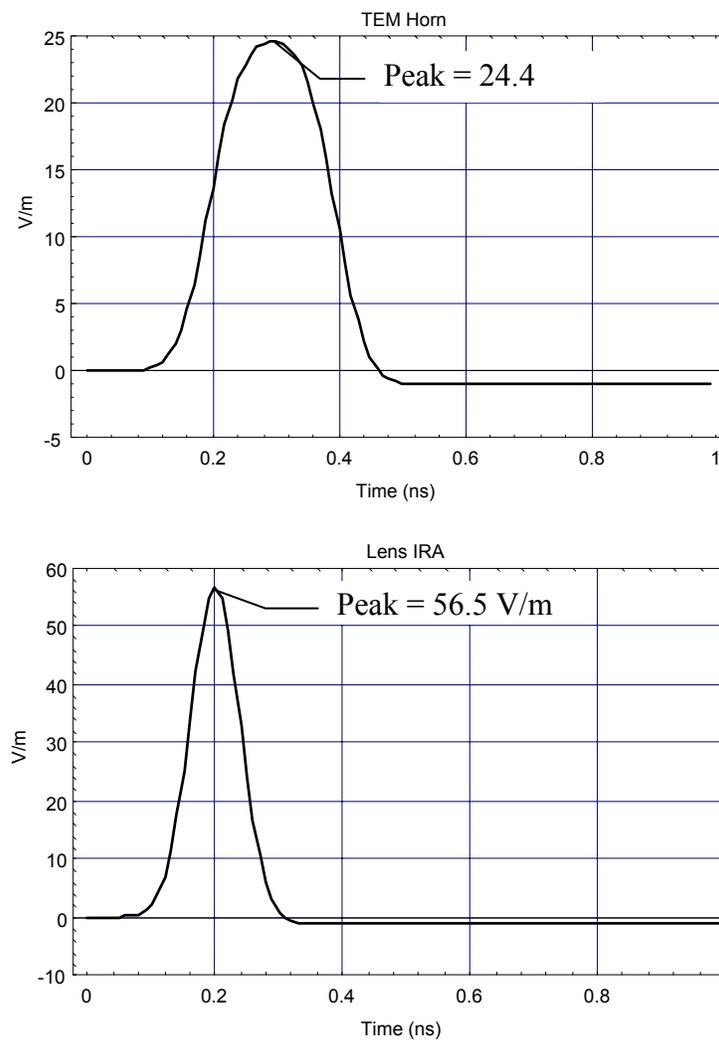

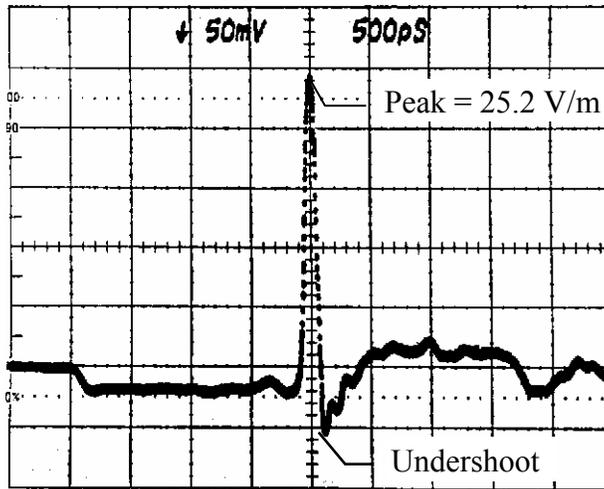Figure 4.2. Predicted response for the TEM horn (top), and Lens IRA (bottom).

Figure 4.3 Experimental results for the reflector IRA. Note that the scales are 500 ps/division horizontal and 50 mV/division vertical. Since the effective height of the sensor is 0.95 cm, this corresponds to a vertical scale of 5.26 V/m/division.
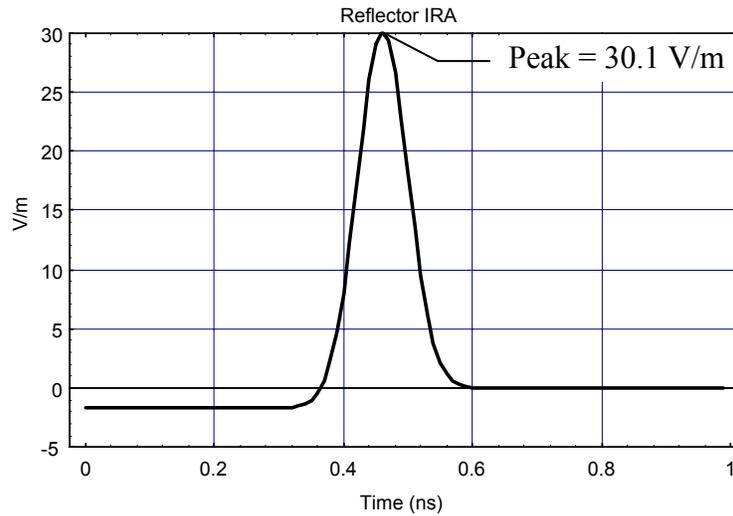

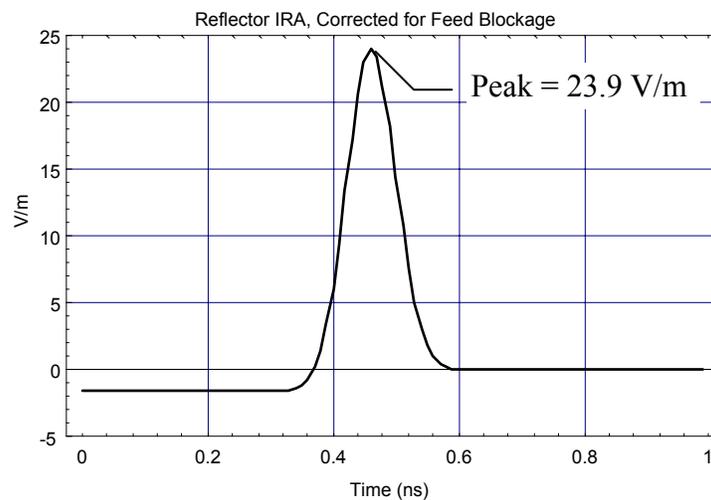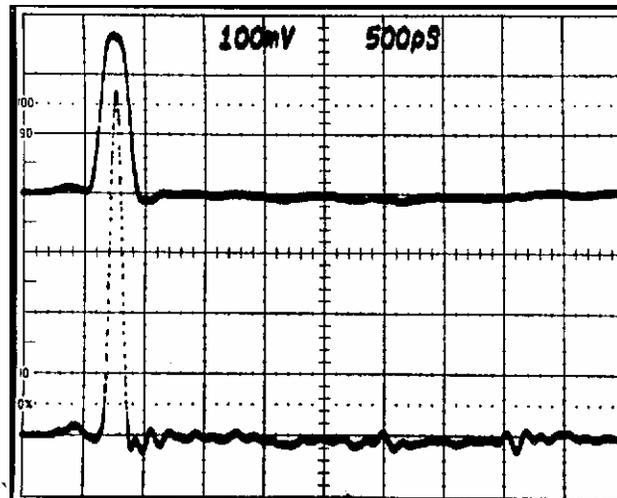Figure 4.4. Predicted results for the reflector IRA.

Figure 4.5. Reflector IRA predictions corrected for feed blockage.

No aperture plate

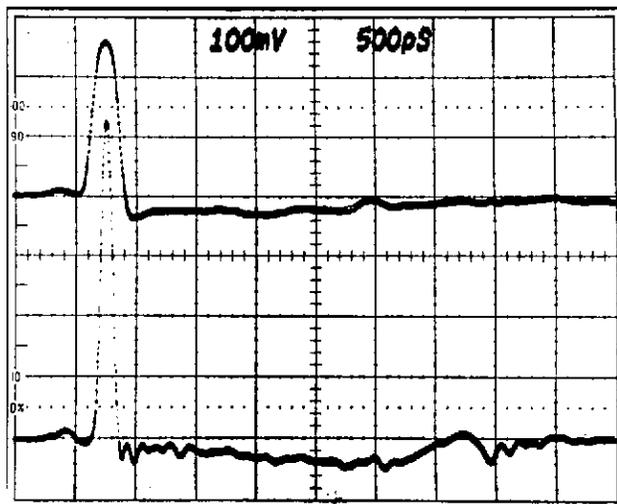TEM Horn

Lens IRA

With aperture plate

TEM Horn

Lens IRA

Figure 4.6. A Comparison of TEM horn and Lens IRA responses with and without the aperture plate. The aperture plate seems to make little difference at early times.

VI.   Conclusions and Recommendations for Future Work

In this note we have reported the results of experiments on reflector and lens IRAs, and on TEM horns. We have compared our results to the theories that have been developed over the past few years, and good agreement is observed between experiment and theory.

Future experiments could be used to investigate a number of issues. First, it would be useful to study the effect of the matching circuit at the end of the feed arms. This may be a difficult experiment because the effects of the matching circuit will be best seen at very late times (low frequencies). Thus, a large antenna range is required to see these effects.

Second, it would be useful to investigate the effect of using a coplanar feed rather than the facing plates used here. Coplanar feed arms should help reduce the feed blockage, as predicted in [11].

One of the reasons why lens IRAs are less practical than reflector IRAs for large apertures is the weight of the polyethylene lens. A low-weight dielectric material or an artificial dielectric (of fine grain) would help this problem, if one were available.

Finally, the replicating sensor used in the measurements here is still a somewhat new design, and further experiments to verify its behavior would be useful.

References

1.   C. E. Baum and E. G. Farr, " Impulse Radiating Antennas," in *Ultra Wideband/Short-Pulse Electromagnetics*, edited by H. L. Bertoni et al, Plenum Press, New York, pp. 139-147, 1993.

2.   C. E. Baum, Radiation of Impulse-Like Transient Fields, Sensor and Simulation Note 321, November 1989.

3.   C. E. Baum, Configurations of TEM Feed for an IRA, Sensor and Simulation Note 327, April 1991.

4.   C. E. Baum, Aperture Efficiencies for IRAs, Sensor and Simulation Note 328, June 1991.

5. E. G. Farr, Analysis of the Impulse Radiating Antenna, Sensor and Simulation Note 329, July 1991.

6. C. E. Baum, General Properties of Antennas, Sensor and Simulation Note 330, July 1991.

7. E. G. Farr and C. E. Baum, Prepulse Associated with the TEM Feed of an Impulse Radiating Antenna, Sensor and Simulation Note 337, March 1992.

8. E. G. Farr and C. E. Baum, A Simple Model of Small-Angle TEM Horns, Sensor and Simulation Note 340, May 1992.

9. E. G. Farr and C. E. Baum, Extending the Definitions of Antenna Gain and Radiation Pattern Into the Time Domain, Sensor and Simulation Note 350, November 1992.

10. C. E. Baum, Circular Aperture Antennas in Time Domain, Sensor and Simulation Note 351, November 1992.

11. E. G. Farr, Optimizing the Feed Impedance of Impulse Radiating Antennas, Part I: Reflector IRAs, Sensor and Simulation Note 354, January 1993.

12. E. G. Farr and C. E. Baum, Radiation from Self-Reciprocal Apertures, Sensor and Simulation Note 357, April 1993.

13. E. G. Farr and C. E. Baum, The Radiation Pattern of Reflector Impulse Radiating Antennas: Early-Time Response, Sensor and Simulation Note 358, June 1993.

14. C. E. Baum, Limited-Angle-of-Incidence and Limited-Time Electric Sensors, Sensor and Simulation Note 359, June 1993.

15. C. E. Baum, et al, Electromagnetic Field Distribution of the TEM Mode in a Symmetrical Two-Parallel-Plate Transmission Line, Sensor and Simulation Note 219, April 1975.

16. T. K. Liu, Impedances and Field distributions of Curved Parallel-Plate Transmission Line Simulators, Sensor and Simulation Note 170, February 1973.